Characterization of aerosol spatial distribution and optical properties over the Indian Ocean from airborne LIDAR and radiometry during INDOEX'99

Jacques Pelon, Cyrille Flamant, Patrick Chazette, J.-F. Leon, D. Tanre, M. Sicard, S. K. Satheesh

Characterization of aerosol spatial distribution and optical properties over the Indian Ocean from airborne LIDAR and radiometry during INDOEX'99

J. Pelon,[1] C. Flamant,[1] P. Chazette,[2] J.-F. Leon,[2] D. Tanre,[3] M. Sicard,[1] and S. K. Satheesh[4]

Received 24 January 2001; revised 25 November 2001; accepted 5 December 2001; published 2 October 2002.

[1] The three-dimensional structure and the optical properties of the Indian pollution plume has been investigated from airborne LIDAR and radiometric measurements over the Indian Ocean during three consecutive days (7, 8, and 9 March 1999) of the INDOEX'99 intensive field phase. The vertical structure of the plume consisted of two layers: the marine atmospheric boundary layer (MABL) and the so-called land plume aloft. The depth of the land plume was observed to depend on the history of the air masses; shallow plumes were associated with air masses coming from the Gulf of Bengal, while deeper plumes were associated with air masses coming from the Indian subcontinent. The larger aerosol optical depths (AODs) observed with Meteosat-5 over the Arabian Sea were associated with the deeper land plume. A combination of airborne light detection and ranging (LIDAR) measurements and Sun photometer measurements at Kaashidhoo Observatory and in Male were used to determine the column-equivalent backscatter-to-extinction ratio needed to retrieve aerosol extinction coefficient profiles and AOD from LIDAR measurements. Direct aerosol forcing was analyzed using a simple radiative model as well as LIDAR-derived AOD and visible flux measurements. Average values of the vertically integrated single scattering albedo of about 0.85 ± 0.05 and 0.8 ± 0.1 were found to be associated with the shallower and the deeper part of the land plume, respectively. *INDEX TERMS:* 0305 Atmospheric Composition and Structure: Aerosols and particles (0345, 4801); 0345 Atmospheric Composition and Structure: Pollution—urban and regional (0305); 1630 Global Change: Impact phenomena; 1640 Global Change: Remote sensing; *KEYWORDS:* Aerosol plume, aerosol optical properties, airborne lidar, radiometry, Sun photometer, INDOEX

Citation: Pelon, J., C. Flamant, P. Chazette, J.-F. Leon, D. Tanre, M. Sicard, and S. K. Satheesh, Characterization of aerosol spatial distribution and optical properties over the Indian Ocean from airborne LIDAR and radiometry during INDOEX'99, *J. Geophys. Res.*, *107*(D19), 8029, doi:10.1029/2001JD000402, 2002.

1. Introduction

[2] The analysis of the direct radiative forcing of aerosols at the global scale requires a better knowledge of pollution aerosol production and transport at the regional scale. Source strengths and modification of aerosol chemical properties during transport need to be better understood. Experiment such as the Transport of Aerosols and Radiative Forcing Experiment (TARFOX), [*Russell et al.*, 1999] and the second Aerosol Characterization Experiment (ACE-2), [*Raes et al.*, 2000] have been previously conducted in the Northern Hemisphere for such a purpose.

[3] Important sources of aerosols linked to human activity exist over the Indian continent and Asia. The analysis of their properties has become an important target of recent research field to better understand and model their chemical modification and radiative impact at the regional scale. During the Indian Ocean Experiment (INDOEX) Intensive Field Phase (IFP), held during the 1999 winter monsoon period, several platforms were used to quantify aerosol composition, stratification and transport, and retrieve their microphysical, chemical and optical properties [J. Coakley et al., unpublished manuscript, 2001; *Ramanathan et al.*, 1995, 2001]. Besides the need to better understand physical processes to better model them, there is a need to directly measure the optical properties of aerosols and retrieve their direct and indirect radiative forcing to constrain models. Indeed, one of the most important parameter in the analysis of aerosol direct radiative forcing is the single scattering albedo (SSA). Measured values in the Northern Hemisphere during TARFOX and ACE-2 are close to 0.9 [*Russell et al.*,

[1]Service d'Aeronomie/IPSL, Universite Pierre et Marie Curie, Paris, France.
[2]Laboratoire des Sciences du Climat/IPSL, Gif-sur-Yvette, France.
[3]Laboratoire d'Optique Atmospherique, Universite des Sciences et Technologies de Lille, Villeneuve d'Ascq, France.
[4]Scripps Institution of Oceanography, University of California, La Jolla, CA, USA.

0148-0227/02/2001JD000402

1999]. Depending on its value and on the aerosol optical depth (AOD), the forcing can be modified by tens of W m^{-2} at the regional scale impacting the vertical structure of the atmosphere [*Leon et al.*, 2001a]. Due to the increase in scattering associated with the presence of aerosol particles in the atmosphere, laser remote sensing provides the unique capability of observing their vertical distribution over any surface. Indeed, airborne light detection and ranging (LIDAR) systems have been used recently to derive their spatial extent as well and derive their optical properties in pollution outbreaks [e.g., *Ferrare et al.*, 2000; *Flamant et al.*, 2000].

[4] The Mystere 20 (M20, IGN/CNRS/CNES/Meteo-France) participated to the INDOEX'99 IFP from 25 February to 15 March 1999, for a total of 6 flights. It was equipped with upward/downward longwave and shortwave radiometers and the backscatter LIDAR LEANDRE 1 (CNRS/IPSL) along with standard in situ sensors. LEANDRE 1 [*Pelon et al.*, 1990] allowed observations of the aerosol vertical structure and optical properties at 532 nm. Dual polarization operation is performed at 532 nm. The objective was to characterize the three-dimensional structure and the optical properties of the Indian pollution plume over the Indian ocean and analyze aerosol forcing from combined active and passive remote sensing. Flights were made around noon (local time) to allow radiation measurements to be taken at high solar elevation. The instruments operated on board the M20 are described in J. Coakley et al. [unpublished manuscript, 2001].

[5] The present analysis focuses on M20 flights performed on 7, 8 and 9 March 1999 during an outbreak event to document the spatial distribution of aerosol north of the Male area, which was under the influence of northeasterly winds bringing polluted air over the ocean. A short description of the meteorological conditions is given in section 2. The spatial structure of the aerosol is presented in section 3. The inversion procedure required to retrieve extinction coefficient profiles from LIDAR measurements is presented in section 4. Spatial distribution of LIDAR-derived AODs are given in section 5 and compared with satellite observations. In section 6, these results are combined with simultaneous shortwave flux measurements to estimate North-South variations of aerosol direct radiation forcing.

2. General Circulation Pattern Associated With the Winter Monsoon: Background and 7–9 March 1999 Case Study of INDOEX

2.1. Background

[6] During the second half of the INDOEX IFP (mid-February to late March), a high pressure area was located over the north-western part of the Indian continent and a low pressure system was over western Indonesia [*Rasch et al.*, 2001]. The synoptic conditions favored northeasterly winds over the Indian Ocean north of the intertropical convergence zone (ITCZ) which was located between the equator and about 10S during INDOEX [*Ramanathan et al.*, 2001]. In such conditions, continental aerosols, both natural and anthropogenic, can be transported over the clean ocean areas hundreds and thousands of kilometer away from sources [*Krishnamurti et al.*, 1998; *Manghnani et al.*, 2000; *Ramanathan et al.*, 2001].

[7] Recent studies have evidenced the key role of elevated plumes in exporting the continental aerosols over the open ocean in pollution outbreak conditions during ACE-2 [*Flamant et al.*, 2000; *Ansmann et al.*, 2000] and TARFOX [*Ferrare et al.*, 2000]. In the particular case of the Indian continental plume during the winter monsoon, the long-range transport of large aerosol loads is regularly observed to reach offshore distances of 600 to 700 km. Several factors, specific to the northeast monsoon flow, can be invoked: the strong near-surface northerly flow, bringing dry continental air over the ocean, as well as subsidence associated with northeasterly monsoon flow lead to low level temperature inversion, mostly clear skies with scattered cumuli and minimal rain, all of which enable the pollution haze to accumulate and spread over the ocean. Northeasterly winter monsoonal flow can transport aerosols from the Indian subcontinent to the ITCZ in a few days depending on its location and shape. This has also been shown to have an impact on the interhemispheric transports via eddies wrapping around the ITCZ [*Krishnamurti et al.*, 1998].

[8] The dry monsoon initiates the buildup of the haze over the Indian subcontinent as evidenced by the seasonal cycle of the aerosol optical depth (AOD) and aerosol burden over the western coast of India observed at Goa and Dharwad [*Leon et al.*, 2001]. AOD measurements evidenced an increase from 0.1 in the premonsoon period to 0.9 by the end of the northeast monsoon period (late March). Typical AOD values for pristine air masses (i.e., such as those found south of the ITCZ) are on the order of 0.1 or less. AODs in excess of 0.2 are indicative of polluted air [*Ramanathan et al.*, 2001]. Eventually, the pollution is transported as far as the island of Kaashidhoo in the Republic of the Maldives (Figure 1, also indicated as Male, capital of the Maldives, in Figure 2) which is about 700 km away from the Indian subcontinent, where the AOD seasonal cycle is also observed [*Ramanathan et al.*, 2001; *Welton et al.*, 2002].

[9] The structure of the ABL over the Indian Ocean during the northeasterly monsoon period has been depicted by *Manghnani et al.* [2000]. The factors responsible for its spatiotemporal variability have been analyzed, among which the proximity of land and the ITCZ. In the vicinity of land, the ABL consists of a shallow marine atmospheric boundary layer (MABL), between the surface and 800 m above sea level (ASL), and an elevated plume of dry continental air aloft. The depth of the MABL was also observed to be quite variable due to the complex nature of the land-sea breeze interactions with the offshore flow [*Manghnani et al.*, 2000].

[10] *Krishnamurti et al.* [1998] suggested that the thickness of the elevated land plume transported over the ocean may be controlled by the diurnal variability of the ABL above land and the height of the trade wind inversion layer. Sea and land breezes are coastal phenomena that further modulate the depth of the continental and marine ABLs, and hence the transport of aerosol. Additionally, the Western Ghats (a mountain ridge of moderate height) along the western coast of India has a profound influence on the structure of the land plume [*Mohanty et al.*, 2001; *Roswintiarti et al.*, 2001; *Leon et al.*, 2001]. Mesoscale simulations of a typical INDOEX IFP sea-breeze event during the daytime show that the near-surface flow from the sea

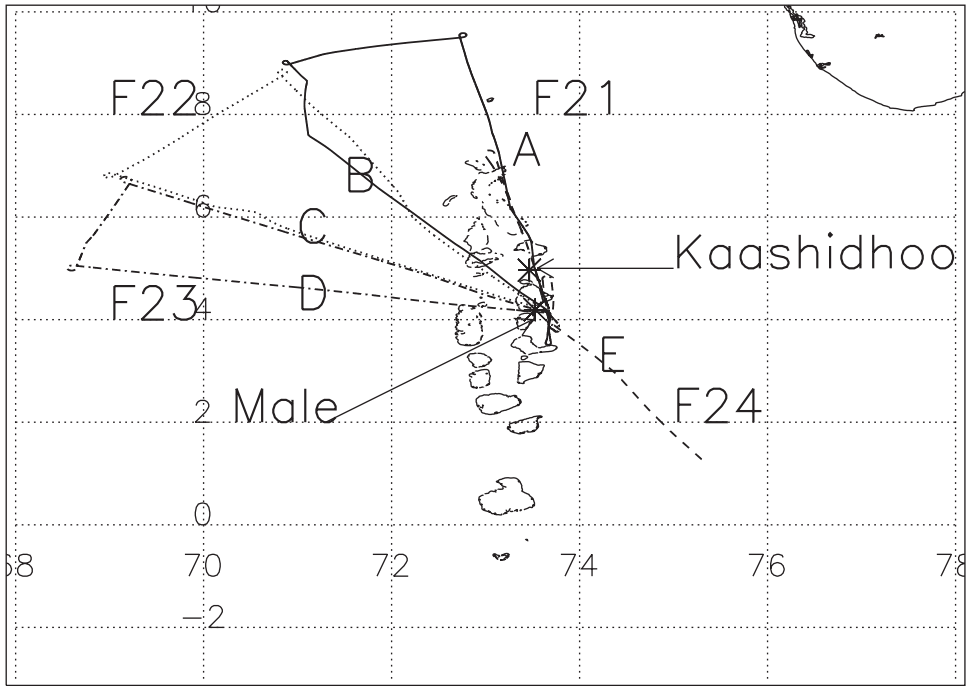

Figure 1. Flight patterns performed on March 7 (F21, thick solid line), March 8 (F22, thick dotted line) and March 9 (F23, thick dash-dotted line) and (F24, thick dashed line) over the Indian Ocean. The F24 pattern composed of half of leg A and leg E.

extends all the way to the Western Ghats, ≈100–150 km inland, where it is forced to flow over the obstacle. In the process, clouds form due to orographic forcing and convergence with the northeasterly synoptic flow. At this point, the continental ABL is well developed on the vertical, sometimes extending as high as 4 km ASL, and continental aerosols are generally observed to be mixed on the vertical throughout the depth of this land plume [*Leon et al.*, 2001].

[11] During the INDOEX IFP, the diurnal cycle of the monsoon ABL (i.e., MABL and land plume) depth has been evidenced by ship-borne LIDAR measurements made on board the R/V *Ronald Brown* [*Welton et al.*, 2002]. The influence of this diurnal variability on the optical properties of the continental plume has been evidenced on Meteosat scenes in the form of westward propagating cloud bands ahead of the pollution plume expelled from the Indian subcontinent as well as frontal discontinuities in the brightness surface temperature fields (Desalmand et al., Westward propagating cloud bands over the Arabian Sea during INDOEX, observed on Meteosat-5 data, unpublished manuscript, 2001), the smaller brightness surface temperatures being observed in a swath approximately parallel to the coastline, over the Arabian Sea.

2.2. Monsoonal Flow During the 7 to 9 March 1999 Period and Aircraft Flight Tracks

[12] Four flights have been performed by the M20 between 7 and 9 March 1999. The corresponding flight patterns (shown in Figure 1) were described counter clockwise. At least one leg was repeated from one flight to the next, to enable comparisons of the vertical distribution of the aerosol in the monsoonal flow, namely in the MABL and aloft. During that series of flight, the northernmost (southernmost) region of the monsoon flow was sampled by the LIDAR on board the M20 aircraft on 7 March 1999 (9 March 1999).

[13] In Figure 2 we show the isentropic back trajectories ending in Male and in the northernmost end-point of the first M20 leg at 0500 UTC on 7 March 1999. Back trajectories were computed using the HYSPLIT4 (HYbrid Single-Particle Lagrangian Integrated Trajectory) Model (courtesy of NOAA Air Resource Laboratory- http://www.arl.noaa.gov/ready/hysplit4.html). In both cases, the flow at 400 m ASL (in the MABL) was from the north whereas the flow aloft was from the northeast as previously reported for winter monsoon flows [e.g., *Krishnamurti et al.*, 1998]. The air masses associated with the land plume over Male had traveled at least 5 days over the ocean from the Gulf of Bengal (offshore of the Indian subcontinent east coast) where pollution haze is also generally observed to build up during the winter monsoon period [*Ramanathan et al.*, 2001]. Back trajectories ending at the northernmost end-point of the M20 leg on 7 March 1999 indicate that the air masses sampled in that region had traveled for the Indian subcontinent for three days prior to being advected over the sea. In Figure 3 we show the isentropic back trajectories ending in Male and in the southernmost end-point of the second M20 leg at 1000 UTC on 9 March 1999. In both locations, and at all levels (between the surface and 2 km ASL), the flow was from the northeast and air masses had traveled from the Gulf of Bengal prior to being advected over the region sampled by the LIDAR on board the M20 aircraft.

[14] The buildup of the haze over the Arabian Sea and the Gulf of Bengal can be observed on the average AOD derived from Meteosat-5 (herein MAOD) at a wavelength of 550 nm for the three days considered (Figure 4). The

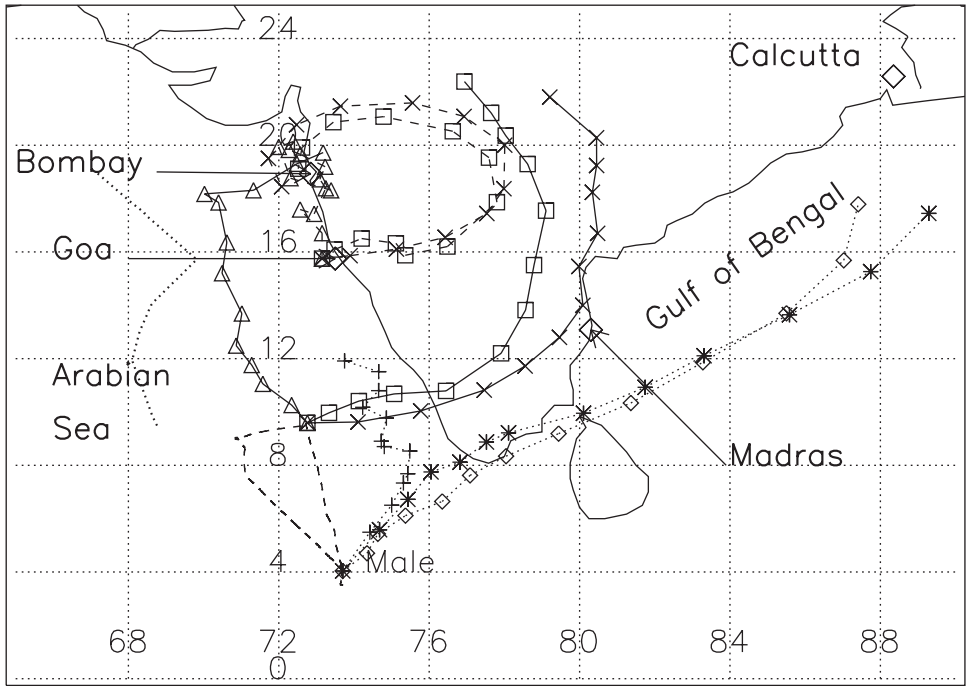

Figure 2. Isentropic back trajectories starting on 2 March 1999, 0500 UTC and ending at Male (dotted lines) on 7 March 1999, 0500 UTC. The trajectories describe the aerosol transport at about 400 m ASL (+), 800 m ASL (∗) and 2000 m ASL (◇). Also shown are the isentropic back trajectories starting on 2 March 1999, 0500 UTC and ending at Goa (dashed lines) and at 9.6°N/72.76°E (solid lines), which corresponds to the northern most part of the plume sampled with the airborne LIDAR LEANDRE 1, on 7 March 1999, 0500 UTC. In both cases, the trajectories describe the aerosol transport at about 400 m ASL (△), 1500 m ASL (□) and 2500 m ASL (×). The dashed line represents the M20 pattern described on 7 March 1999 (F21). The thick dotted line represents the track of the R/V *Ronald Brown* from 7 to 9 March 1999 (south to north).

MAOD field is a composite of the daily averaged AOD field for 7, 8 and 9 March 1999. White pixels correspond to clouds. Only clouds that are persistent enough to have been observed at the same location during the 3 days are presented as such. In the other cases, the AOD is taken as the average of the non cloudy pixels. Large values of MAOD (above 0.4) are observed to extend over the Arabian Sea as far as 700 km from the coast. AOD values larger than 0.4 appeared to be confined to the north of 8°N, which also corresponds to the tip of the Indian subcontinent. South of 8°N, the MAOD decreases from 0.4 to 0.2 or less. Large AODs are also observed over the Gulf of Bengal.

3. Airborne LIDAR Observations of the Aerosol Spatial Distribution

[15] The attenuated backscatter coefficient, ABC (the product of the total (molecules and particles) backscatter coefficient of a given atmospheric layer and the two-way transmission between the aircraft and that layer) is used to depict the horizontal and vertical structure of the aerosol plume over the Indian ocean. Figures 5 through 7 show the 2D LIDAR cross-sections of the ABC obtained along legs A, B and C, respectively (see Figure 1). The decrease in ABC near the surface (see, for example, Figure 5 at latitudes north of 8°N or in the presence of clouds at the top of the MABL) is related to lower two-way transmission values above these regions (i.e., aerosol or cloud scattering).

[16] The vertical structure of the monsoon consisted of two layers: the MABL and the so-called land plume aloft. Numerous cumulus clouds were observed at the top of the MABL as well as embedded in the land plume. Such clouds may be considered as mixing elements between the MABL and the upper layer. These clouds eventually feed deeper clouds at the ITCZ [*Manghnani et al.*, 2000]. The depth of the MABL varied between 0.3 and 0.7 km ASL over the course of the 3 days both as a function of time and space, and was somewhat smaller than the MABL top height measurements obtained, during the same period, with the micropulse LIDAR system on board the R/V *Ronald Brown* (0.72 ± 0.25 km ASL) [*Welton et al.*, 2002] west of the M20 measurements (the track of the ship is shown as the thick dotted line Figure 2). Such variability, in the vicinity of the land was shown to be due to the complex nature of the land-sea breeze interactions with the offshore flow [*Manghnani et al.*, 2000].

[17] The depth of the land plume also exhibited large fluctuations both in time and space during the three days. LIDAR observations on 7 and 8 March 1999 evidence 3 regions:

1. A deep plume region: the land plume was observed to be deepest north of 8° N (Figures 5a and 6). The height of the top of the land plume was located at 3 km ASL on 7 March 1999 (Figures 5a and 6a), and at 2.5 km ASL on 8 March 1999 (Figure 6b). In this region, the height of the land plume top did not vary much along the M20 aircraft tracks. The height of the top of the land plume deduced

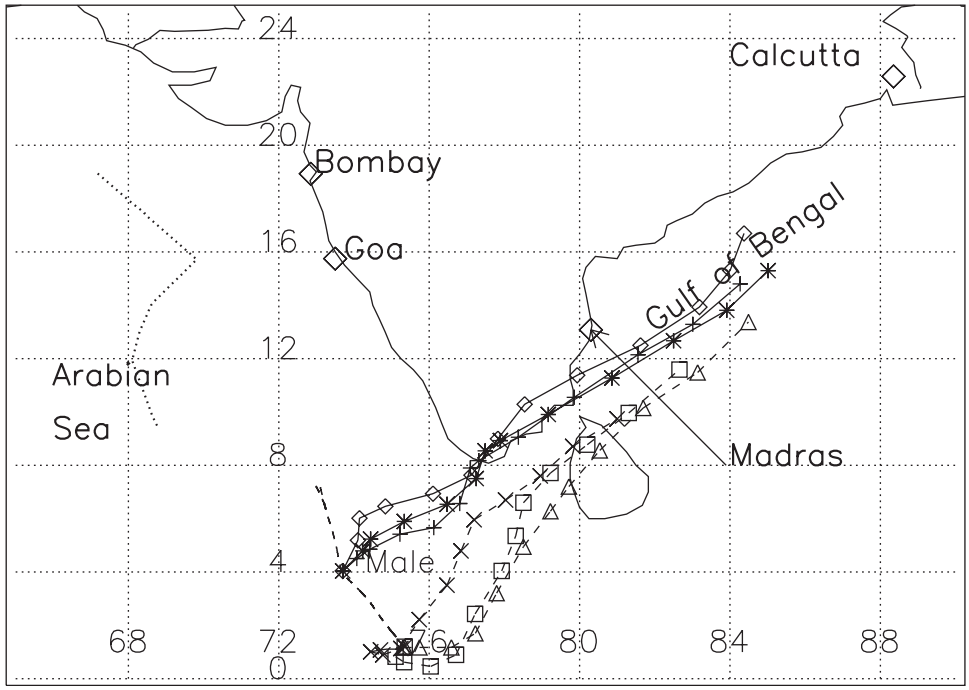

Figure 3. Isentropic back trajectories starting on 4 March 1999, 1000 UTC and ending at Male (solid lines) on 9 March 1999, 1000 UTC. The trajectories describe the aerosol transport at about 400 m ASL (+), 800 m ASL (∗) and 2000 m ASL (◇). Also shown are the isentropic back trajectories starting on 4 March 1999, 1000 UTC and ending at 1.2°N/75.35°E (dashed lines), which corresponds to the southern most part of the plume sampled with the airborne LIDAR LEANDRE 1, on 9 March 1999, 1000 UTC. The trajectories describe the aerosol transport at about 400 m ASL (△), 800 m ASL (□) and 2000 m ASL (×). The dashed line represents the M20 pattern described on 9 March 1999 (F24).The thick dotted line represents the track of the R/V *Ronald Brown* from 7 to 9 March 1999 (south to north).

from LIDAR measurements was close to the temperature inversion height observed at 4 km ASL from radiosonde data in Goa (15.75°N) (not shown). It also is in fair agreement with the land plume top height measurements obtained, during the same period, with the micropulse LIDAR system on board the R/V *Ronald Brown* (3.48 ± 0.23 km ASL) [*Welton et al.*, 2002]. The lower land plume top height observed by LEANDRE 1 further offshore can be explained by subsidence, as it is usually important over the sea during winter monsoon.

2. A transition region: between 8°N and 6°N, the land plume top height decreased drastically with latitude from 2.5–3 km ASL to 1.5 km ASL (Figures 5a, 6, 7).

3. A shallow plume region: the land plume was observed to be most shallow south of 6°N (Figures 5a, 6, and 7). The height of the land plume top of the land plume was located at 1.5 km ASL on both days. In this region also, the height of the land plume top did not vary much along the M20 aircraft tracks. In this region, the LIDAR-derived MABL and land plume height top coincided exactly with the two temperature inversions evidenced in the soundings performed during M20 take-offs from and landings in Male. Soundings over Male also revealed that the relative humidity (RH) varied between 60 and 80% near the surface, reaching values of 95% or more at the MABL top. Above, in the land plume, RH was found to be on the order of 40%, except near the top of this layer where RH increased sharply to 80%, as generally observed in winter monsoonal flows [e.g. *Mohanty et al.*, 2001; *Manghnani et al.*, 2000].

[18] According to back trajectory analyses, the air masses composing the elevated plume south of 6°N were coming from the Gulf of Bengal, whereas the air masses composing the deeper part of the plume (north of 8°N) were coming from the Indian subcontinent (Figure 2). The transition region then appears as a region of mixing between two adjacent air masses with different history. Hence, it appears that the larger MAODs observed with Meteosat-5 (Figure 4) over the Arabian Sea are associated with the deeper land plume coming from the Indian subcontinent. Conversely, the smaller MAODs are associated with the shallower land plume from the Gulf of Bengal.

[19] On 9 March 1999 (Figure 5b), the land plume depth was nearly constant between 7°N and 2.5°N. On that day, the monsoon flow sampled by LIDAR was almost entirely coming from the Gulf of Bengal (Figure 3). Simultaneously, the MABL depth was observed to deepen from 0.4 to 0.8 km between 7°N and 2.5°N. South of 2°N, the land plume takes the form of a faint elevated aerosol layer.

4. Retrieval of Aerosol Optical Properties in the Vicinity of KCO From Combined LIDAR and Sun Photometer Analysis

[20] Using the molecular scattering in the upper clean air, the total optical thickness of aerosol and the vertical

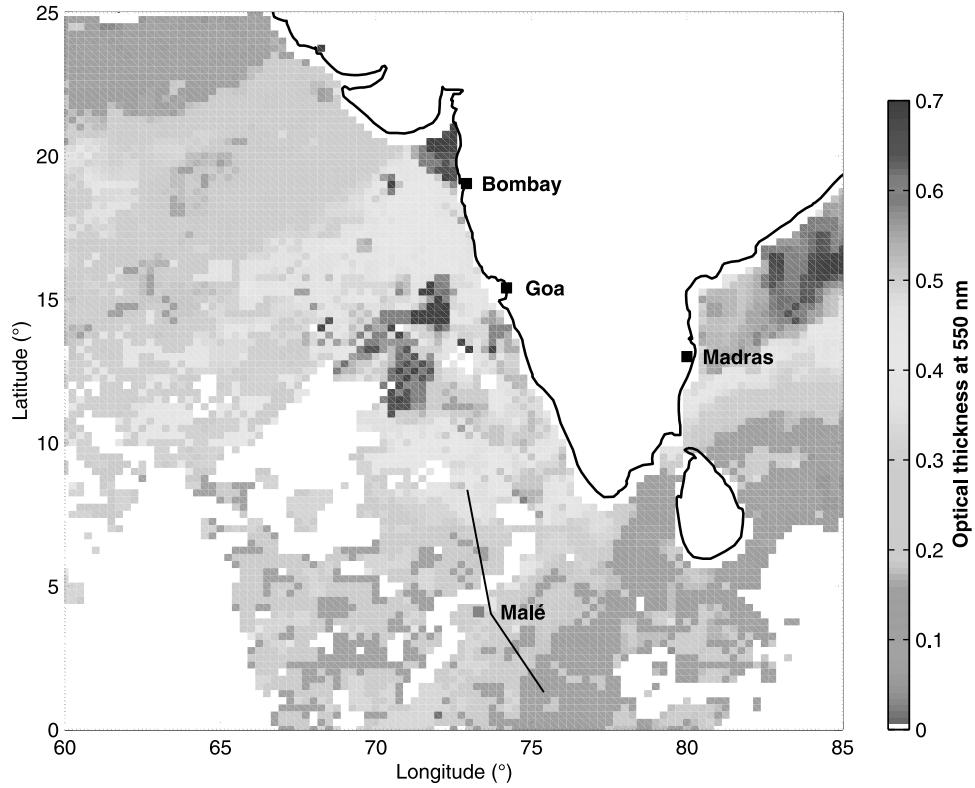

Figure 4. Average AOD derived from Meteosat-5 for the three days considered. The AOD field is a composite of the daily averaged AOD field for 7, 8 and 9 March 1999. White pixels correspond to clouds. Only clouds that are persistent enough to have been observed at the same location during the 3 days are presented as such. In the other cases, the AOD is taken as the average of the non cloudy pixels. The thick solid line represents track A and track E (north and south of Male, respectively) flown by the M20 on 7 March 1999 and 9 March 1999, along which Meteosat-5 AODs shown in Figure 10 have been extracted.

extinction profile can be retrieved from airborne LIDAR data using the Klett inversion procedure in a forward calculation mode [*Klett*, 1985]. However for an accurate inversion of the LIDAR signal, the value of the backscattering-to-extinction ratio (BER), k_p, must be known. It is to be emphasized that since the LIDAR equation is obtained from the radiative transfer equation with a geometry specific to LIDAR observations, k_p is equal to the product of the normalized aerosol phase function at an angle of 180° corresponding to backscattering of the aerosol and the SSA ω_0. Hence, k_p depends on both the size distribution and the nature of the aerosol as a function of height. We will show here that values of k_p are similar in the MABL and in the monsoon layer, and

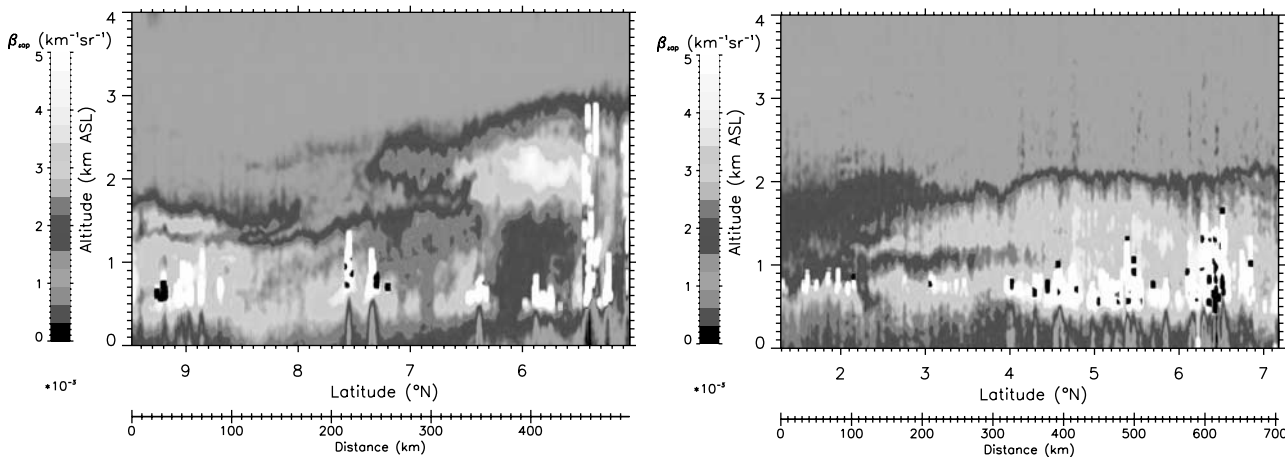

Figure 5. Lidar-derived ABC obtained at 532 nm by LEANDRE 1 along track A on (a) 7 March 1999 and (b) on 9 March 1999. The later also includes measurements made on track E. The distance covered is also indicated.

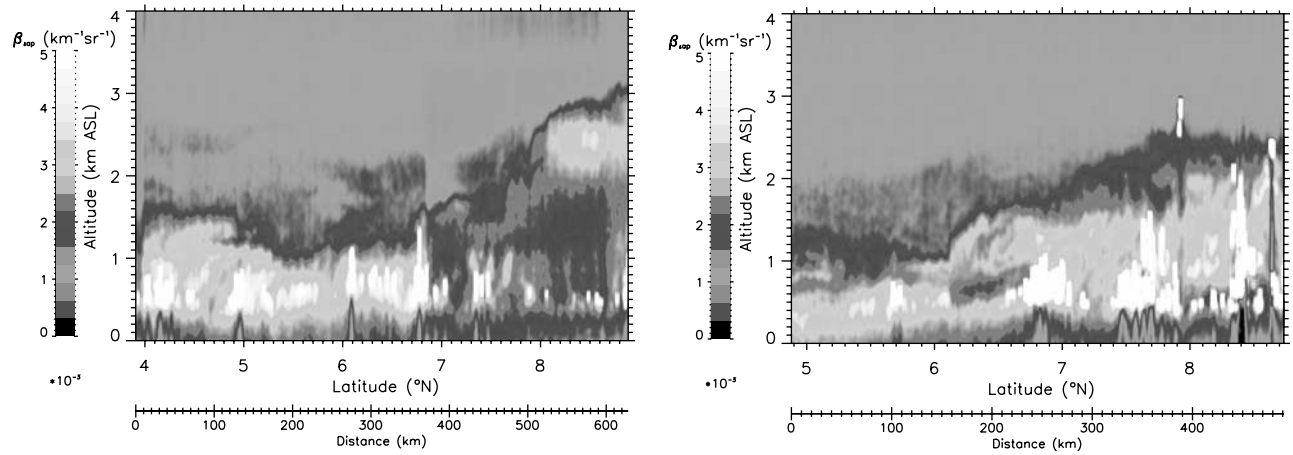

Figure 6. Same as Figure 5 but for track B on (a) 7 March 1999 and (b) on 8 March 1999.

that a single layer approach can be used to retrieve the total AOD.

[21] AOD measurements using CIMEL Sun photometers were taken on Male Island near the airport and on Kaashidhoo Island about 50 km north of Male. Measurements at Kaashidhoo Climate Observatory (KCO) are part of the AErosol RObotic NETwork (AERONET) which is a monitoring network at the global scale [*Holben et al.*, 1998]. Outside of winter monsoon periods, this Observatory is located in a very pristine environment. It is operational since 1998 and has already allowed first characterization of Indian aerosol prior to INDOEX IFP [*Satheesh et al.*, 1999]. Measurements in Male were acquired specially for the INDOEX IFP. In the present study we used Sun photometer AODs (SAODs) measured at 440, 500 and 670 nm. SAODs measured at 500 nm were corrected from the wavelength dependence estimated using the three channels to retrieve the SAOD at the LIDAR wavelength (532 nm). A comparison of the SAODs measured by the two Sun photometers in Male and KCO revealed them to be comparable on a statistical basis. The slope of the regression between measurements is 0.90 ± 0.05. However the dispersion is high (about 30%) showing that the fluctuations are important at a scale of a few tens of kilometers. These fluctuations are thought to reflect the variability of the long-range transport of haze to the Maldives. Back trajectory analyses indicate that the Maldives are under the influence of air masses coming from both the north at low levels (Arabian Sea) and from the east (Gulf of Bengal) as shown by Figures 2 and 3. Depending on synoptic scale circulation patterns, the measurements in either Male and KCO will reflect the characteristics of the incoming air mass. Furthermore, differences in the AOD observed at the two sites could also be due to local circulations such as wake effects and/or land/sea breezes [*Manghnani et al.*, 2000]. In the following, we have used both Male and KCO data in the analysis, depending on the proximity and availability of the data.

4.1. Integrated Column Analysis

[22] The M20 made overpasses of Male and KCO during all flights which allowed comparisons between airborne LIDAR and Sun photometers measurements. AODs corresponding to these overpasses are reported in Table 1. Lidar-derived extinction coefficient profiles are first obtained using a constant value of k_p with altitude in the forward Klett algorithm [*Klett*, 1985]. For each of the Male or KCO overpass, a series of 15 cloudless LIDAR profiles (closest to the ground site) representative of a horizontal distance of 30 km are selected. Simultaneously, cloudy Sun photometer data (large SAODs and/or small Angstrom coefficients at

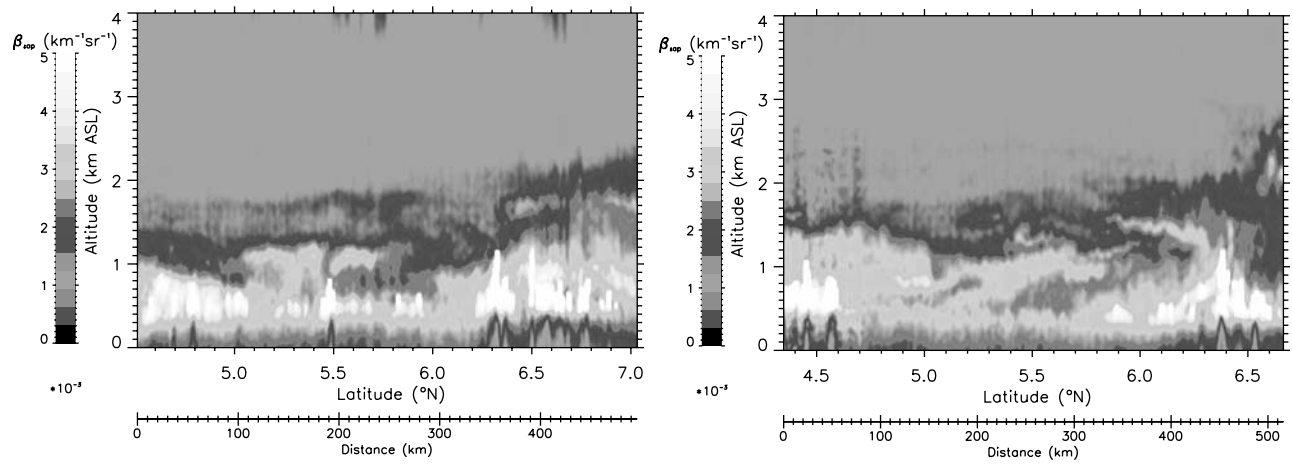

Figure 7. Same Figure 5 but for track C on (a) on 8 March 1999 and (b) on 9 March 1999.

Table 1. Sun Photometer Aerosol Optical Depth (AOD) in KCO on 7, 8, and 9 March 1999[a]

	Time, UTC	Sun Photometer AOD	BER Column sr^{-1},	BER MABL, sr^{-1}
Day				
7 March 1999	0342–0345	0.435	0.013	0.013
	0613–0614	0.435	0.013	0.013
8 March 1999	0354–0356	0.280	0.012	0.013
	0619–0622	0.290	0.010	0.010
9 March 1999	0416–0418	0.310	0.010	0.011
	0633–0635	0.310	0.012	0.013
	1000–1002	0.460	0.012	0.013
Average			0.0115	0.012
Standard deviation			0.001	0.001

[a] AOD values are given at 532 nm. The corresponding backscatter-to-extinction ratio (BER) derived from 15 LIDAR profiles acquired in the vicinity of the Kaashidhoo Climate Observatory are also given for the integrated column and the 2-layer approaches. In the 2-layer approach, the value of the BER in the land plume is assumed to be between 0.0095 and 0.015 sr^{-1}, and the BER values shown below correspond to BER in the MABL. For the set of data considered in this study, a worst case estimate of the uncertainty associated with the BER is ±0.001 sr^{-1}. The uncertainty associated with Sun photometer AODs is ±0.02.

532 nm) are discarded. In the LIDAR inversion procedure, k_p varied between 0.005 and 0.045 sr^{-1}, and an average LIDAR-derived AOD (LAOD) is calculated for 15 selected profiles. We then select the value of k_p for which the average LAOD best matches the corresponding SAOD. The uncertainty on k_p is the quadratic sum of two terms: (1) the uncertainty resulting from the natural variability associated with the data, which is calculated as the standard deviation of the BER computed for each individual profiles, and (2) the uncertainty associated with the uncertainty on the SAOD, i.e., ±0.02 [*Hamonou et al.*, 1999]. For the set of data considered in this study, a worst case estimate of the uncertainty associated with the BER is 0.001 sr^{-1}.

[23] The sensitivity of the LAODs and the LIDAR-derived extinction coefficient profiles to the value of the BER is illustrated in Figures 8 and 9, respectively, for measurements made at the end of leg B on 7 March 1999. It is seen in Figure 8 that the AOD increase as the value of k_p is reduced, due to the increase of the extinction coefficient throughout the profile (Figure 9). This behavior is due to the increasing contribution of the transmission at low k_p. The dashed line in Figure 8 represents the SAOD (0.435) measured by the KCO Sun photometer shortly before the M20 landing on 7 March 1999. The dotted lines represent the uncertainty associated with this measurement (±0.02). The value of k_p which allows the LIDAR observations to match the Sun photometer measurements in the present case is 0.013 ± 0.001 sr^{-1}. Values of k_p obtained for the 4 flights considered in this study are listed in Table 1. The uncertainty associated with LAOD retrievals is on the order of 15%.

[24] Daily values of the BER have also been derived from the Sun photometer measurements in Male. The spectral measurements of direct and diffuse radiation performed by the sun-sky scanning radiometers of AERONET [*Holben et al.*, 1998] are used to simultaneously derive the aerosol size distribution and the complex refractive index [*Dubovik and King*, 2000]. It has been shown that the retrieval accuracy is quite acceptable [*Dubovik et al.*, 2000] except for dust particles that require specific analysis since the Mie theory does not apply to nonspherical particles.

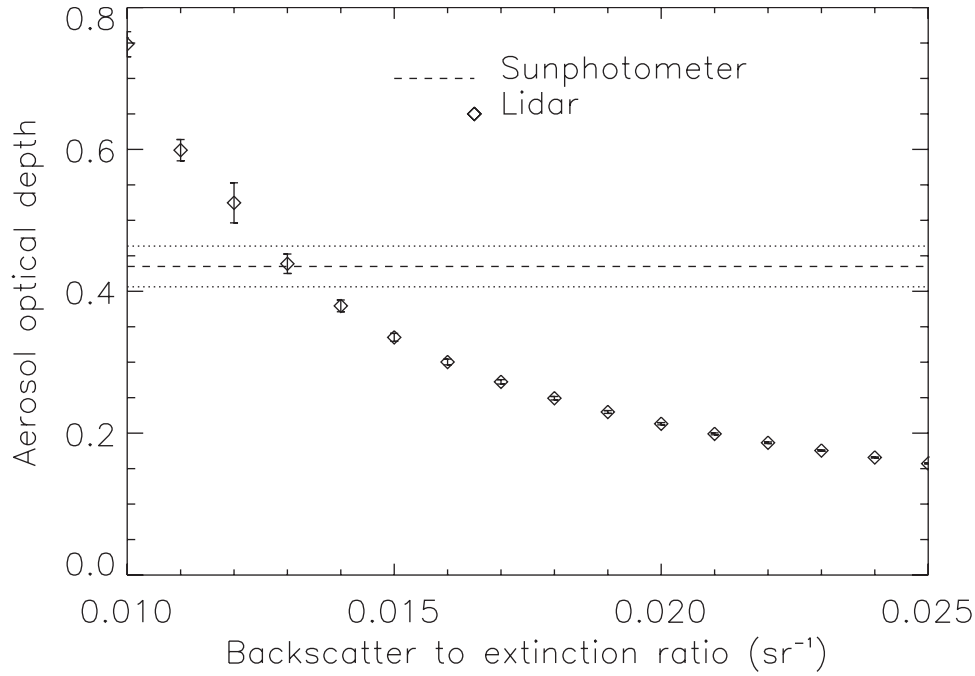

Figure 8. Average LIDAR-derived AOD at 532 nm as a function of the backscatter-to-extinction ratio from 15 LIDAR profiles acquired in the vicinity of KCO on 7 March 1999. Error bars are the standard deviation associated with the 15 profiles for the different k_p values. The dashed line represents the AOD (0.435) measured by the KCO Sun photometer shortly before landing on 7 March 1999. The dotted lines represent the uncertainty associated with such measurement (±0.02).

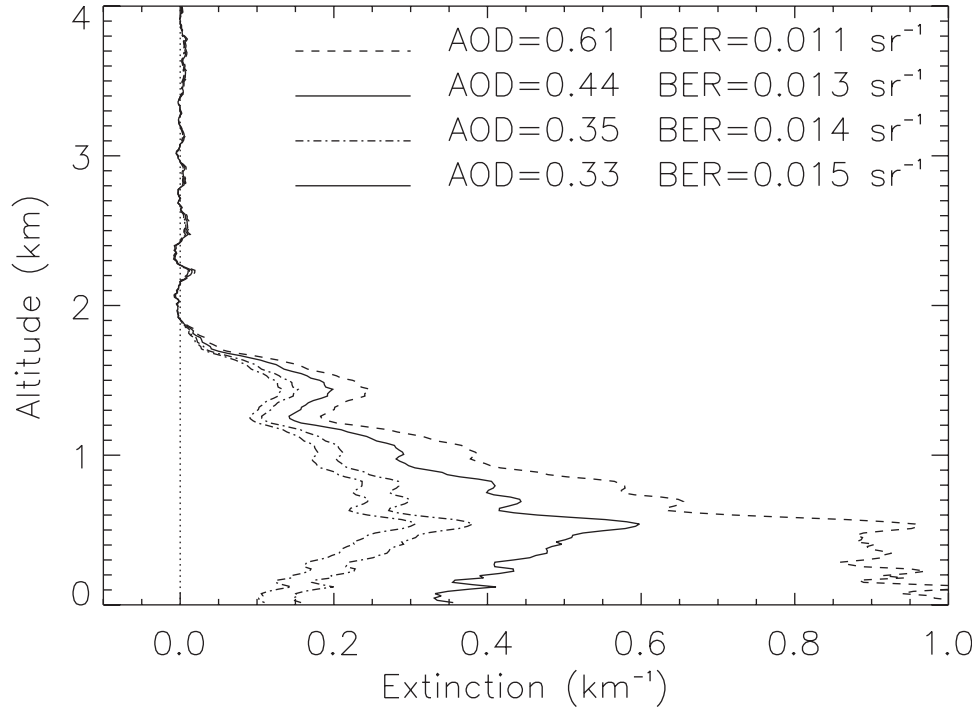

Figure 9. Lidar-derived extinction coefficient profiles obtained for different values of the backscatter-to-extinction ratio (BER) assumed constant with height. The total aerosol optical thickness corresponding to the vertical profile is reported for the different BER used.

Once the physical parameters of the aerosols are known, i.e., size distribution, complex refractive index and shape (hereafter spherical), the optical parameters that are not directly measured like the BER or the asymmetry parameters can be derived. In our case, we found BER values of 0.012, 0.014 and 0.015 sr^{-1} on 7, 8 and 9 March 1999, respectively. These values are in good agreement with those derived from combined LIDAR-photometer measurements reported in Table 1. The uncertainty associated these measurements is due to the uncertainty on the retrieval of the particle volume size distribution. In particular, for the intermediate particle range (0.1–7 μm), characteristic of the continental aerosol advected over the Arabian Sea during the IFP, the retrieval errors do not exceed 10% [*Dubovik et al.*, 2000]. The uncertainty on BER retrievals from Sun photometer is taken as 10%.

[25] During the 3-day period, the LAODs derived in the KCO/Male area often were observed to vary by a factor of 2, while the retrieved value of k_p did not fluctuate by more than 10% around the average value of 0.0115 sr^{-1}. This factor of 2 variation on the SAOD was observed both in Male and KCO. Lidar measurements revealed that on days when the SAODs were low (as for example on 8 March 1999), the LIDAR-derived extinction in the land plume was also very low (i.e., evidencing a cleaner land plume), so that the difference in both LAODs and SAODs observed between 7 and 8 March 1999 results from the contribution of the land plume. However, even for days characterized by small LAOD/SAODs, the value of k_p was still small (less than 0.015 sr^{-1}) and comparable to those obtained for days characterized by larger LAOD/SAODs. The low values of k_p observed reflect the fact that the SSA may also be much smaller than in the aerosol outbreaks previously observed in Northern Hemisphere, as may be expected from a higher content in carbonaceous aerosol.

4.2. Two-Layer Analysis

[26] The value of k_p retrieved with the single column approach is really an "equivalent" k_p representative of properties in the MABL and in the land plume. However, carbonaceous aerosol (organics and soot from pollution), sea-salt, non sea-salt water soluble, non absorbing condensed organic phases (Particulate Organic Matter, POM), and mineral dust which are the main components of the aerosol phase over the Indian Ocean [*Jayaraman et al.*, 1998; *Satheesh et al.*, 1999; *Alfaro et al.*, 2001] may be distributed differently in the two aerosol layers. Interestingly though, these constituents were observed in surface measurements made in Goa [*Alfaro et al.*, 2001] and Male [*Satheesh et al.*, 1999]. This advocates for long range transport in the MABL and/or downward mixing from the land plume into the MABL over the Maldives.

[27] Two recent studies by *Ansmann et al.* [2000] and *Leon et al.* [2001] indicate that, during the INDOEX IFP, the BER above the MABL was on the order of that derived from the integrated column approach in the previous section. *Ansmann et al.* [2000] reported BER vertical profile measurements made in Male on 25 March 1999 (under similar synoptic conditions), with a multiple wavelength LIDAR system. The BER values derived above the MABL ranged between 0.0095 and 0.013 sr^{-1}. In the other study, the aerosol model used by *Leon et al.* [2001] to derive the MAOD from Meteosat-5 radiances, based on aerosol size distribution measurements at the surface in Goa [*Alfaro et al.*, 2001], yields a value between 0.012 and 0.015 sr^{-1}. This model is defined as a monomodal log-normal distribution

Table 2. Three-Day Average of the Backscatter-to-Extinction Ratio (BER) and Aerosol Asymmetry Parameter Measured in Goa and in the Male/Kaashidhoo Area from Different Platforms and Instruments[a]

	BER, sr^{-1}			g	
Location	Lidar	Photometer	Meteosat	Photometer	Meteosat
Goa	0.032/0.015[b]	0.017–0.022	0.012–0.015[c]	0.65–0.70	0.55 ± 0.03[c]
Male/KCO	0.010–0.013	0.012–0.015	0.012–0.015	0.64–0.68	0.55 ± 0.03

[a] For the set of data considered in this study, a worst case estimate of the uncertainty associated with the LIDAR derived BER is ±0.001 sr^{-1}. The uncertainty associated Sun photometer measurements (asymmetry factor g and BER) is due to the uncertainty on the retrieval of the particle volume size distribution and is taken as 10% (see section 6).
[b] In Goa, the BER was estimated to be equal to 0.032 sr^{-1} between 0.5 and 1.5 km and equal to 0.015 sr^{-1} between 2 and 3 km [*Sicard et al.*, 2001].
[c] From *Leon et al.* [2001].

characterized by an average mean diameter of 0.12 μm and a dispersion of 1.78 ± 0.06. This mode corresponds to the smaller of the 3 modes generally identified in this region [*Jayaraman et al.*, 1998; *Satheesh et al.*, 1999; *Alfaro et al.*, 2001] and is composed of soot particles coated with POM along with non sea-salt sulphates [*Alfaro et al.*, 2001]. The "equivalent" refractive index characterizing the haze over the sea is tuned so that MAODs match SAODs measured in different locations (Goa, KCO and on board the R/V *Ronald Brown*) [*Leon et al.*, 2001]. The best fit is obtained for an "equivalent" refractive index of 1.43-*i* 0.03, at ambient RH (≈60%). This value is in agreement with that derived in other regions of the globe for continental aerosol outbreaks [*Anderson et al.*, 1996; *Flamant et al.*, 1998, 2000]. However, note that because of the observation angles (150–160°), MAODs are not very sensitive to the aerosol model employed.

[28] In the MABL, over the open ocean or in coastal regions not subject to anthropogenic influence, k_p is generally calculated from Mie theory to be on the order of 0.035 to 0.045 sr^{-1} [*Flamant et al.*, 1998, 2000; *Ackerman*, 1998]. In the present study, a sensitivity analysis has been conducted in which both the BER in the MABL and in the land plume are allowed to vary between 0.005 and 0.045 sr^{-1}. The LAOD is calculated for each possible combination of BER pairs ($k_{p,MABL}$; $k_{p,ML}$) considered as solutions whenever the LAOD and the SAOD agree within 10%. In this analysis, we imposed an additional constraint: the LIDAR-derived extinction coefficient should not exceed 0.8 km^{-1} in the lower troposphere, above the surface layer. This corresponds to a surface visibility (from the M20) of 5 km, as estimated by eye in clear air over Male area during the 3-day period. The BER values retrieved in the MABL are close to the one obtained with a single layer analysis (Table 1), that is much smaller than those generally found in marine air masses and MABLs. These values are also very close to those considered in the land plume and obtained in the integrated column analysis. This suggests that the integrated column approach is relevant to study the aerosol optical properties of the Indian plume, as done in the following section.

5. Optical Depth Analysis

[29] The purpose of this section is to investigate the evolution of the AOD in Indian plume between 1°N and 9.6°N, along tracks A and E on 7 and 9 March 1999. As shown from back trajectory analyses given in Figure 2, it is doubtful that the BER derived in Male can be used to derive LAOD north of 8°N. This is further emphasized by the difference between the BER determined from Sun photometer measurements in Goa and Male (Table 2). During the days of interest, the BER in Goa, as obtained from Sun photometer measurements, is 50% larger than in Male (0.017 vs 0.0125 sr^{-1} and 0.022 vs 0.0115 sr^{-1} on 7 and 9 March 1999, respectively). In the following, we have used the 3-day average value of LIDAR-derived k_p derived in the previous section (0.0115 sr^{-1}, Table 1) in the region south of 8°N. North of 8°N, we used an increased value of the BER corresponding to the upper limit derived in KCO during the 3-day period (0.013 sr^{-1}, Table 1). This value was selected as being intermediate between the BER values derived in the Male/KCO area and in northwestern India (Bombay and Goa areas). Figure 10 shows the results obtained during the south-to-north transect corresponding to Figure 5. Error bars correspond to LAOD obtained with ± one standard deviation (±0.001 sr^{-1}, Table 1). Cloudy LIDAR profiles were discarded using a threshold value on the backscatter coefficient (the magnitude of signal backscattered by clouds is on the order of 2 to 10 times the signal backscattered by particles). Nevertheless, large LAODs can still be observed (north of 9°N) which are due to an inadequate cloud screening (i.e., cloud edges).

[30] The MAOD was observed to increase with latitude from 0.1 near 1°N (characteristic of pristine air) to 0.4 near 4.5°N, in the Male/KCO area. Large values of MAOD in the region of the Maldives are related to transport from the Gulf of Bengal as discussed earlier. Such an increase was also observed on the LAOD retrievals, even though not as marked. LAOD values increased slightly from 0.2 to 0.25 (on average) between 1°N and 3.5°N. In the region of the Maldives, persisting cumulus clouds prevented significant LAOD retrievals. Nevertheless, LAOD values as large as 0.4 were observed near 4.75°N. Between 4.75°N and 5°N, a large decrease was observed in both the LAOD and the MAOD. Finally, north of 5°N, the LAOD and MAOD were observed to steadily increase from an average value of 0.2 to a value of 0.45 near 9°N. Values of LAOD larger than 0.4 are found north of 8°N which corresponds to the deep plume region (Figure 5a). Note that these larger values are not due to the larger BER value used in this region (i.e., 0.013 sr^{-1}): as discussed in section 4, a larger BER leads to a smaller AOD in the LIDAR inversion procedure. When using a BER value of 0.0115 sr^{-1} in the LIDAR inversion procedure, LAODs north of 8°N can reach 0.8, which is much larger than those obtained with Meteosat and retrieved from AVHRR [*Collins et al.*, 2001]. Finally, the LAODs are found larger than the Meteosat AODs by as

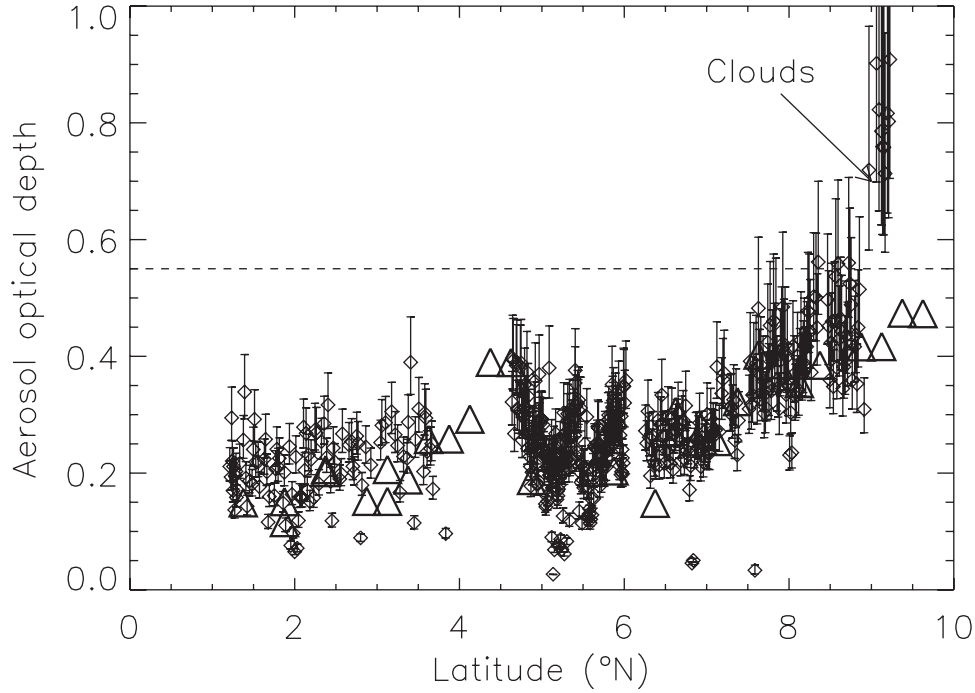

Figure 10. Lidar-derived AOD on 7 March 1999 (south-to-north transect corresponding to Figure 5a using a BER value of 0.0115 sr^{-1} (0.013 sr^{-1}) south (north) of 8°N. Error bars correspond to LAOD obtained with a ±0.001 uncertainty on the BER. Open triangles correspond to AODs extracted from average AOD field derived from Meteosat-5 along this axis. The dashed line represents the boundary (0.55) above which LAODs are assumed to be contaminated by cloud edges and discarded.

much as 0.05, on average. This discrepancy can be explained by the difference in the wavelength of observation. It could be also caused by errors in LIDAR and Meteosat-5 data analyses.

6. Radiative Forcing

[31] The aerosol SSA can be estimated from simultaneous measurements of AOD and the "equivalent" albedo of the layer, defined as the upward visible flux divided by the downward visible flux. Whenever these measurements are performed from an airborne platform (as it is the case here), the evolution of the value of the aerosol SSA with the distance from the continent can be investigated. The albedo could be obtained on leveled legs (i.e., without pitch and roll correction) from measurements made by the two Eppley radiometers installed on board the M20 [*Saunders et al.*, 1992].

[32] Figure 11 shows the albedo as a function of LAOD on track A for 7 March 1999. On this track, large values of albedo and upward visible flux at 5.5°N and 9.5°N (not show) were caused by the presence of clouds (Figure 5a). Cloud contaminated albedo measurements were discarded assuming values of upward visible flux larger than 100 W m^{-2} were caused by the presence of clouds. Referring to results obtained in the previous section, only LAOD values smaller than 0.55 have been used in this analysis (dashed line in Figure 10). The albedo increased from a value of 0.05 in the shallow plume region to a value of nearly 0.09 in the deep plume region. The aerosol SSA was estimated by looking for trends comparable to those observed for albedo versus AOD relationships computed in the framework of the two-stream approximation [*Irvine*, 1968]. In this model we have assumed a single aerosol layer (e.g., a layer close to the surface with homogeneous microphysical and optical properties). This somewhat coarse assumption may be justified by the fact that BER values in the MABL and in the land plume were found to be very similar. The asymmetry factor g was taken equal to 0.69, i.e., the average value obtained from Sun photometer measurements in Male and Goa for the 3-day period (Table 2). The uncertainty on g is taken as 10%. Computations were made at solar elevations corresponding to the time and latitude of the airborne observations. For a first analysis, we selected the Practical Improved Flux Method method developed by *Zdunkowski et al.* [1980], which was shown to be accurate for optical thickness smaller than 1.0, intermediate solar zenith angles (40°) and moderate absorption. The absolute and relative accuracies remain respectively better than 0.005 and 10% for our observation conditions [*Zdunkowski et al.*, 1980].

[33] The integrated SSA on 7 March 1999 was observed to evolve with latitude. South of 8°, it is about 0.85 ± 0.05 (i.e., between the curves for $\omega_0 = 0.8$ and $\omega_0 = 0.9$, Figure 11a). North of 8°, the SSA is about 0.8 ± 0.1 (i.e., between the curves for $\omega_0 = 0.7$ and $\omega_0 = 0.9$, Figure 11b). This value is in fair agreement with the value of 0.83 ± 0.04 found by [*Leon et al.*, 2002].

7. Summary and Conclusion

[34] The three-dimensional structure and the optical properties of the Indian pollution plume has been investigated from airborne LIDAR and radiometric measurements over the Indian Ocean during three consecutive days (7, 8 and 9 March 1999) of the INDOEX'99 Intensive

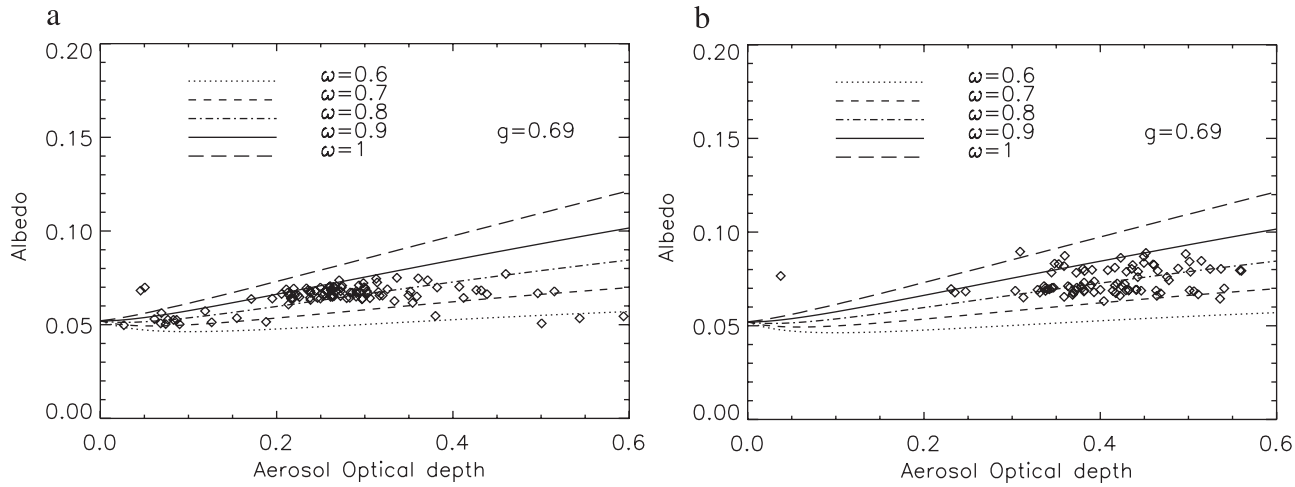

Figure 11. Variation of the observed and modeled albedo as a function of the aerosol optical thickness. Diamonds correspond to observations using radiometry (albedo) and LIDAR (AOD) on 7 March 1999. Panel (a) and panel (b) are observations south and north of 8°N, respectively. The lines represent the relationships between albedo and AOD modeled (for different values of ω_0) using the two-stream approximation for a value of $g = 0.69$. The short-dashed, dot-dashed, 3-dot-dashed and long-dashed lines correspond to single scattering albedos of 0.7, 0.8, 0.9 and 1, respectively.

Field Phase. The vertical structure of the plume consisted of two layers: the marine atmospheric boundary layer (MABL) and the so-called land plume aloft. The depth of the MABL as well as the depth of the land plume varied significantly with latitude and time. On 7 March 1999, a deep plume (top at about 3 km ASL) was observed north of 8°N, while south of 6°N a shallow plume (top at about 1.5 km ASL) was observed. Back trajectory analyses evidence that the air masses composing the elevated plume south of 6°N were coming from the Gulf of Bengal, whereas the air masses composing the deeper part of the plume (north of 8°N) were coming from the Indian subcontinent. The transition region, between 6°N and 8°N appeared as a region of mixing between two adjacent air masses with different history. The larger aerosol optical depths observed with Meteosat-5 (MAODs) over the Arabian Sea were associated with the deeper land plume. A similar behaviour was observed on 8 March 1999. However, the land plume north of 8°N was not as deep as on 7 March 1999 (top at about 2.5 km ASL). On 9 March 1999, the land plume depth was nearly constant between 7°N and 2.5°N. On that day, the monsoon flow sampled by LIDAR was almost entirely coming from the Gulf of Bengal.

[35] Sun photometer aerosol optical depth (SAOD) measurements performed at Kaashidhoo Observatory and in Male were used to determine the column-equivalent backscatter-to-extinction ratio (the inverse of the so-called LIDAR ratio) needed to retrieve aerosol extinction coefficient profiles and AOD from LIDAR measurements. This ratio was found to range between 0.010 and 0.013 sr^{-1}, in good agreement with other studies and values derived independently from Sun photometer measurements. A sensitivity study (in which two layers, a MABL and a land plume, are considered) evidenced the backscatter-to-extinction ratio to be comparable in the MABL and the land plume, which indicates that the MABL is still subject to anthropogenic pollution as far as 700 km from the Indian coastline, and that it is more polluted (i.e., characterized by a smaller value of the BER) further offshore than it is near the coast. Interestingly, the BER values derived from airborne LIDAR measurements in the MABL were in excellent agreement with those reported by *Sicard et al.* [2001] in Goa between 2 and 3 km ASL on 10 March 1999. *Sicard et al.* [2001] also reported BER values of 0.032 sr^{-1} between 0.5 and 1.5 km in Goa. Hence the picture arises that the aerosol particles expelled from the continent in the land plume gets mixed into the MABL during the transport over the ocean which explains the relatively close BER values derived from LIDAR in the MABL and aloft. Shallow cumulus clouds as well as clear air entrainment at the MABL top due to the advection of continental air above the MABL [*Manghnani et al.*, 2000] may be considered as mixing elements between the MABL and the upper layer.

[36] The LIDAR derived AODs (LAODs) measured during the 3-day period varied between 0.2 at southernmost latitudes (1°N) and 0.4 in the northernmost part of the studied area (9.6°N). These values are in good agreement with the values obtained from Meteosat data analysis. On 7 March 1999, direct aerosol forcing is analyzed using a simple radiative model in which a single aerosol layer is considered. Simultaneous measurements of the LAOD and equivalent albedo (from radiometry) lead to an average value of the vertically integrated SSA of about 0.85 ± 0.05 near Male (associated with the shallower part of the land plume) and 0.8 ± 0.1 at the northernmost latitudes (associated with the deeper part of the land plume). Provided that the difference is not solely due to the uncertainty on the retrieval technique, the SSA values on 7 March 1999 are smaller than values previously found in pollution outbreaks over the western Atlantic ocean for similar AODs [*Hignett et al.*, 1999], which could mean that the aerosol transported over the Indian Ocean is more absorbing. Interestingly, the lowest LIDAR/radiometry-derived SSA value was not associated with the lowest LIDAR derived BER (recall that the BER is the product of the aerosol phase function and the SSA). This could be related to the nature of

the aerosol transported in the land plume. Back trajectory analyses evidenced that the air masses composing the elevated plume south of 6°N were coming from the Gulf of Bengal, whereas the air masses composing the deeper part of the plume (north of 8°N) were coming from the Indian subcontinent. Hence, the aerosol optical characteristics could be slightly different.

[37] Further investigations of these features will be conducted with the Colorado State University Regional Atmospheric Modeling System (RAMS) model (coupled with an aerosol module) to analyze the three-dimensional distribution of three major types of aerosol observed during the INDOEX IFP, namely black carbon, non sea-salt sulfate and mineral dust, in connection with LIDAR observations.

[38] **Acknowledgments.** Authors would like to acknowledge INSU-CNRS support provided by the Programme National de Chimie Atmospherique and the Programme Atmosphere et Ocean a Moyenne echelle. The authors are indebted to the European Space Agency for their additional support to the Mystere 20 flights. They also wish to express their gratitude to the AERONET team for maintaining the instruments and to Brent Holben for providing the data.

References

Ackerman, J., The extinction-to-backscatter ratio of tropospheric aerosol: A numerical study, *J. Atmos. Ocean. Tech.*, *15*, 1043–1050, 1998.

Alfaro, S., L. Gomes, A. Gaudichet, J. L. Rajot, J. F. Leon, H. Cachier, P. Chazette, and F. Dulac, Modeling of aerosol optical properties at an Indian coastal site during the 1999 INDOEX field phase, *J. Aerosol Sci.*, *32*, S423–S424, 2001.

Anderson, B. E., W. B. Grant, G. L. Gregory, E. V. Browell, J. E. Collins Jr., G. W. Sachse, D. R. Bagwell, C. H. Hugdins, D. R. Blake, and N. J. Blake, Aerosol from biomass burning over the tropical South Atlantic region: Distributions and impacts, *J. Geophys. Res.*, *101*, 24,117–24,137, 1996.

Ansmann, A., D. Althausen, U. Wandinger, K. Franke, D. Müller, F. Wagner, and J. Heitzenberg, Vertical profiling of the Indian aerosol plume with six-wavelength LIDAR during INDOEX: A first case study, *Geophys. Res. Lett.*, *27*, 963–966, 2000.

Collins, W. D., P. J. Rasch, B. E. Eaton, B. V. Khattatov, J.-F. Lamarque, and C. S. Zender, Simulating aerosol using a chemical transport model with assimilation of satellite aerosol retrievals: Methodology for INDOEX, *J. Geophys. Res.*, *106*, 7313–7336, 2001.

Dubovik, O., and M. D. King, A flexible inversion algorithm for retrieval of aerosol optical properties from Sun and sky radiances measurements, *J. Geophys. Res.*, *105*, 20,673–20,696, 2000.

Dubovik, O., A. Smirnov, B. N. Holben, M. D. King, Y. J. Kaufman, T. F. Eck, and I. Slutsker, Accuracy assessments of aerosol optical properties retrieved from aerosol robotic network (AERONET) Sun and sky radiance measurements, *J. Geophys. Res.*, *105*, 9791–9806, 2000.

Ferrare, R. A., et al., Comparisons of LASE, aircraft and satellite measurements of aerosol optical properties, and water vapor during TARFOX, *J. Geophys. Res.*, *105*, 9935–9947, 2000.

Flamant, C., V. Trouillet, P. Chazette, and J. Pelon, Wind speed dependence of atmospheric boundary layer optical properties and ocean surface reflectance as observed by airborne backscatter LIDAR, *J. Geophys. Res.*, *103*, 25,137–25,158, 1998.

Flamant, C., et al., Airborne LIDAR measurements of aerosol spatial distribution and optical properties over the Atlantic Ocean during a European pollution outbreak of ACE-2, *Tellus, Ser. B*, *52*, 662–677, 2000.

Hamonou, E., P. Chazette, D. Balis, F. Dulac, X. Schneider, E. Galani, G. Ancellet, and A. Papayannis, Characterization of the vertical structure of Saharan dust export to the Mediterranean basin, *J. Geophys. Res.*, *104*, 22,257–22,270, 1999.

Hignett, P., J. P. Taylor, P. N. Francis, and M. D. Glew, Comparison of observed and modeled direct aerosol forcing during TARFOX, *J. Geophys. Res.*, *104*, 2279–2287, 1999.

Holben, B. N., et al., AERONET—A federated instrument network and data archive for aerosol characterization, *Remote Sens. Environ.*, *66*, 1–16, 1998.

Irvine, W. M., Multiple scattering by large particles, *Astrophys. J.*, *152*, 823–834, 1968.

Jayaraman, A., D. Lubin, S. Ramachandran, V. Ramanathan, E. Woodbridge, W. D. Collins, and Z. S. Zalpuri, Direct observations of aerosol radiative forcing over the tropical Indian Ocean during the January–February 1996 pre-INDOEX cruise, *J. Geophys. Res.*, *103*, 13,827–13,836, 1998.

Klett, J. D., Lidar inversion with variable backscatter/extinction ratios, *Appl. Opt.*, *24*, 1638–1643, 1985.

Krishnamurti, T. N., B. Jha, J. Prospero, A. Jayaraman, and V. Ramanathan, Aerosol and pollutant transport and their impact on radiative forcing over the tropical Indian Ocean during the January–February 1996 pre-INDOEX cruise, *Tellus, Ser. B*, *50*, 521–542, 1998.

Leon, J.-F., et al., Large-scale advection of continental aerosols during INDOEX, *J. Geophys. Res.*, *106*, 28,427–28,440, 2001.

Leon, J.-F., P. Chazette, J. Pelon, F. Dulac, and H. Ramdriamarisoa, Aerosol direct radiative impact over the INDOEX area based on passive and active remote sensing, *J. Geophys. Res.*, *107*, 10.1029/2000JD000116, in press, 2002.

Manghnani, V., S. Raman, D. Niyogi, V. Parameswara, J. Morrison, S. V. Ramana, and J. Raju, Marine boundary-layer variability over the Indian Ocean during INDOEX (1998), *Boundary Layer Meteorol.*, *97*, 411–430, 2000.

Mohanty, U., D. Niyogi, S. Raman, and A. Sarkar, Numerical simulation of land-air-sea interactions over the Indian ocean during the northeasterly Monsoon during INDOEX, *Curr. Sci.*, *80*, 60–68, 2001.

Pelon, J., P. H. Flamant, and M. Meissonnier, The French airborne backscatter LIDAR LEANDRE 1: Conception and operation, paper presented at the 15th International Laser Radar Conference, Dep. of Gen. Phys. and Astron. of the USSR Acad. of Sci., Tomsk, Russia, 1990.

Raes, F., T. Bates, F. M. McGovern, and M. Van Liederkerte, The second Aerosol Characterization Experiment (ACE-2): General overview and main results, *Tellus, Ser. B*, *52*, 111–126, 2000.

Ramanathan, V., et al., Indian Ocean Experiment (INDOEX), *White Pap. C4*, Scripps Inst. of Oceanogr., Univ. of Calif., San Diego, La Jolla, Calif., 1995.

Ramanathan, V., et al., The Indian Ocean Experiment: An integrated analysis of the climate forcing and effects of the great Indo-Asian haze, *J. Geophys. Res.*, *106*, 28,371–28,398, 2001.

Rasch, P. J., W. D. Collins, and B. E. Easton, Understanding the Indian Ocean Experiment INDOEX aerosol distributions with an aerosol assimilation, *J. Geophys. Res.*, *106*, 7337–7356, 2001.

Roswintiarti, O., D. Niyogi, S. Raman, and U. Mohanty, Application of a three-dimensional triple nested mesoscale model (MM5) for assessing the transport and the boundary layer variability over the Indian Ocean during INDOEX, *Curr. Sci.*, *80*, 69–76, 2001.

Russell, P. B., P. V. Hobbs, and L. L. Stowe, Aerosol and radiative effects in the United States east coast haze plume: An overview of the Tropospheric Aerosol Radiative Forcing Observational Experiment (TARFOX), *J. Geophys. Res.*, *104*, 2213–2222, 1999.

Satheesh, S. K., V. Ramanathan, X. Li-Jones, J. M. Lobert, I. A. Podgorny, J. M. Prospero, B. N. Holben, and N. G. Loeb, A model for the natural and anthropogenic aerosols over the tropical Indian Ocean derived from Indian Ocean Experiment data, *J. Geophys. Res.*, *104*, 27,421–27,440, 1999.

Saunders, R. W., G. Brogniez, J. C. Buriez, R. Meerktter, and P. Wendling, A comparison of measured and modeled broadband fluxes from aircraft data during the ICE'89 field experiment, *J. Atmos. Ocean. Tech.*, *9*, 391–406, 1992.

Sicard, M., P. Chazette, J. Pelon, J. G. Won, and S.-C. Yoon, Variational method for the retrieval of the optical thickness and the backscatter coefficient from multiangle LIDAR profiles, *Appl. Opt.*, *41*, 493–502, 2001.

Welton, E. J., K. J. Voss, P. K. Quinn, P. J. Flatau, K. Markowicz, J. R. Campbell, J. D. Spinhirne, H. R. Gordon, and J. E. Johnson, Measurements of aerosol vertical profiles and optical properties during INDOEX 1999 using micropulse LIDARs, *J. Geophys. Res.*, *107*, 10.1029/2000JD000038, in press, 2002.

Zdunkowski, W. G., R.M. Welch, and G. Korb, An Investigation of the structure of typical two-stream methods for the calculation of solar fluxes and heating rates in clouds, *Contrib. Atmos. Phys.*, *53*, 147–166, 1980.

P. Chazette and J.-F. Leon, Laboratoire des Sciences du Climat, Bât. 709, Orme des Merisiers, F-91191 Gif-sur-Yvette Cedex, France. (pch@lsce.saclay.cea.fr; Leon@univ-lille1.fr)

J. Pelon, C. Flamant, and M. Sicard, Service d'Aeronomie, Universite Pierre et Marie Curie, Boîte 102, 4 place Jussieu, F-75252 Paris Cedex, France. (jpe@aero.jussieu.fr; cyf@aero.jussieu.fr; msi@aero.jussieu.fr)

S. K. Satheesh, Scripps Institution of Oceanography, University of California, La Jolla, CA, USA. (satheesh@fiji.ucsd.edu)

D. Tanre, Laboratoire d'Optique Atmospherique, Bat. P5, Universite des Sciences et Technologies de Lille, F-59655 Villeneuve d'Ascq Cedex, France. (Didier.Tanre@univ-lille1.fr)